

Characterization and optimization of a heterolytic Ring Laser Gyroscope

Nicolò Beverini¹, Giorgio Carelli^{1,2}, Simone Castellano^{*,2,3}, Giuseppe Di Somma^{1,2}, Angela D.V. Di Virgilio², Enrico Maccioni^{1,2}, Paolo Marsili^{1,2}

¹ *Dipartimento di Fisica, Università di Pisa, largo B. Pontecorvo 3, I-56127 Pisa, Italy*

² *Istituto Nazionale di Fisica Nucleare (INFN), sez. di Pisa, largo B. Pontecorvo 3, I-56127 Pisa, Italy*

³ *Gran Sasso Science Institute, Viale Francesco Crispi 7, 67100 L'Aquila AQ, Italy **

(Dated: June 21, 2024)

A characterization of Ring Laser Gyroscopes (RLGs) was performed at INFN-Pisa, and optimization is ongoing for a kind of very high sensitivity and accuracy rotation measurement device. Data quality is monitored through fringe contrast, such quantity is factorized, as it depends on single light beam values and their alignment, and on the polarization of the beams at their interference outside the cavity. Models of the alignment and polarization contributions to contrast have been implemented. In particular, the GP2 prototype at INFN-Pisa was characterized as for non-planarity, alignment, and polarization of the interfering beams. Beams interference was optimized by obtaining linearly polarized beams out of the cavity. Advantage with respect to elliptically polarized interfering beams is shown.

I. INTRODUCTION: THE RING LASER GYROSCOPE AND THE "SAGNAC" SIGNAL

Large area Ring Laser Gyroscopes (RLGs) have the capability of measuring the frame angular velocity in a bandwidth ranging from DC to kHz, with unprecedented sensitivity. The kind of measurement that can be performed with such devices is relevant in many aspects, its scientific fields of interest range from seismology [1] to fundamental physics, such as testing gravitomagnetic effects foreseen by general relativity, (i.e. the Lense Thirring effect), and beyond [2]. A RLG schematic view is shown in Fig.1. Its working principle is based on the Sagnac effect. When the optical cavity of a ring laser is rotating around its axis, the time of round trip of the light beam co-rotating with the cavity is slightly increased, while that of the counter-rotating one is slightly decreased. Then, a small frequency difference is produced between the two beams traveling in the opposite directions. This frequency difference, named Sagnac frequency (f_s), is proportional to the frame rotational velocity Ω and can be observed as the beat note between the two beams on a photo-detector:

$$f_s = \frac{4A}{\lambda L} \Omega \cos(\theta) = S \Omega \cos(\theta), \quad (1)$$

where A is the area defined by the ring cavity, L is its perimeter, λ the wavelength of the light, and θ is the angle between the area vector of the ring and the rotational axis. For RLGs horizontally aligned (area vector vertical) θ is the colatitude angle, while for RLGs aligned at the maximum Sagnac frequency $\theta = 0$. The GP2 and GINGERino RLGs of the GINGER collaboration are both equipped with a double beat-note signal detection, this allows a better signal-to-noise ratio, and deeper analysis procedures. RLG prototypes of the GINGER collaboration are square cavities enclosed by very high reflectivity mirrors. Data are taken from transmitted radiation, we collect the intensities of the two counter propagating beams (I_1, I_2) and two beat note signals (S1,S2), from which the frequency is reconstructed. Such reconstruction is performed by means of the Hilbert transform, which identifies amplitude and phase of the signal. By time deriving the phase term, and multiplying it for the acquisition rate, the measured beat note pulsation (ω_m from here on) is obtained. ω_m is however affected by laser non linear dynamics and some corrections must be done, in order to obtain the true value of $\omega_s = 2\pi f_s$, as reported in [3, 4].

Typical laser disturbances are usually referred to as 'mode jumps' (very fast spikes, they affect data quality for a few seconds, and the measurement of Ω at the level of a few nrad/s) and 'split modes' (these disturbances may last for hours and they impair the measurement of Ω for their whole duration, but can be eliminated by geometry control), typically about 10% of the data are removed in a free running device, when the geometry is controlled the duty cycle is 100%[5]. A good indicator of data quality is fringe Contrast (we will simply refer to it as C), this other observable will be treated in detail and utilized in the present analysis. In Fig.2, we show Ω obtained from the "raw" frequency ω_m with and without selection on the basis of C (above), and C (below).

*Electronic address: simone.castellano@gssi.it, simone.castellano@pi.infn.it

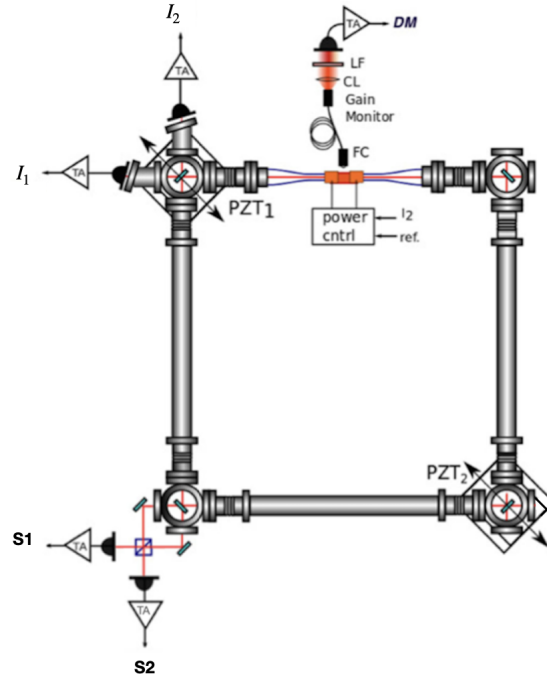


FIG. 1: Schematic view of a typical Ring Laser Gyroscope (RLG). In particular, data acquired are the two laser beam intensities, and two beat note signals.

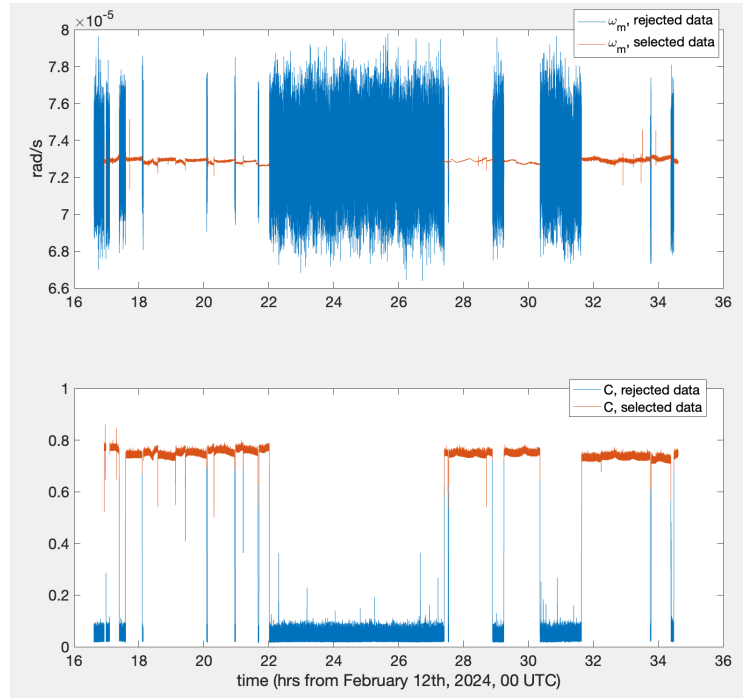


FIG. 2: Ω obtained from ω_m with and without data selection (above), and C (below); how the selection is performed on the basis of C is shown.

Data shown are from GP2, where measurements for the present work were performed; being in a very noisy environment, the duty cycle is rather low. In the present article, we make a characterization of GP2 at INFN-Pisa, and show the improvement obtained by optimizing the beams output. Since the optimization is performed on raw

data, the parameters checked are ω_m , and C. The work is structured as follows: in section 2, the implemented model of fringe Contrast, as function of the beams geometry and polarization, is described in detail. In section 3, we describe the beams polarization measurement for GP2. In section 4, the improvement that is obtained by making the beams linearly polarized at the cavity output is outlined, and a measurement of the GP2 beams off-axis is described.

II. A MODEL OF THE FRINGE CONTRAST

RLGs provide a sinusoidal signal, therefore fringe Contrast is defined as:

$$C = \frac{I_{max} - I_{min}}{I_{max} + I_{min}}, \quad (2)$$

where " I_{max} " and " I_{min} " are the local intensity maxima and minima of the beat note signal.

From light interference, we know that:

$$I_{max} = I_1 + I_2 + 2 \cdot \sqrt{I_1 \cdot I_2} \cdot \eta_{vis} \quad (3)$$

$$I_{min} = I_1 + I_2 - 2 \cdot \sqrt{I_1 \cdot I_2} \cdot \eta_{vis}, \quad (4)$$

where η_{vis} is a coefficient called "visibility"; therefore:

$$C = \frac{I_{max} - I_{min}}{I_{max} + I_{min}} = \frac{2 \cdot \sqrt{I_1 \cdot I_2}}{I_1 + I_2} \cdot \eta_{vis} \quad (5)$$

We can factorize η_{vis} as:

$$\eta_{vis} = \eta_{geom} \cdot \eta_{pol}, \quad (6)$$

where η_{geom} is a contribution arising from the overlapping of the two beams at the point of interference, and η_{pol} is the contribution arising from the polarizations of the two interfering beams.

A. The beams alignment

η_{geom} was derived by considering the interference of two gaussian beams, of identical intensities ($I_1 = I_2$) and geometry, propagating in the same z direction, with their z axes positioned at $y = 0$, $x = \pm k$, being x and y the other two cartesian coordinates, perpendicular to the direction of the beams propagation. The parameter k is the distance between the two beams axes divided by the width of the gaussian beam profiles at $1/e^2$ in intensity. η_{pol} is set to 1, to consider only the geometrical contribution. In such conditions, we have:

$$\eta_{geom} = C = \frac{I_{max} - I_{min}}{I_{max} + I_{min}} \quad (7)$$

Intensity maxima and minima (I_{max} and I_{min}) of the beams interference were calculated as functions of k , therefore η_{geom} was derived. η_{geom} as function of k is shown in Fig.3.

$$I_{max} = \frac{1}{2\pi} \int_{-\infty}^{+\infty} \int_{-\infty}^{+\infty} (e^{-[(x+k)^2+y^2]} + e^{-[(x-k)^2+y^2]})^2 dx dy \quad (8)$$

$$I_{min} = \frac{1}{2\pi} \int_{-\infty}^{+\infty} \int_{-\infty}^{+\infty} (e^{-[(x+k)^2+y^2]} - e^{-[(x-k)^2+y^2]})^2 dx dy \quad (9)$$

From equations 7, 8, and 9, we derive:

$$\eta_{geom} = e^{-2k^2} \quad (10)$$

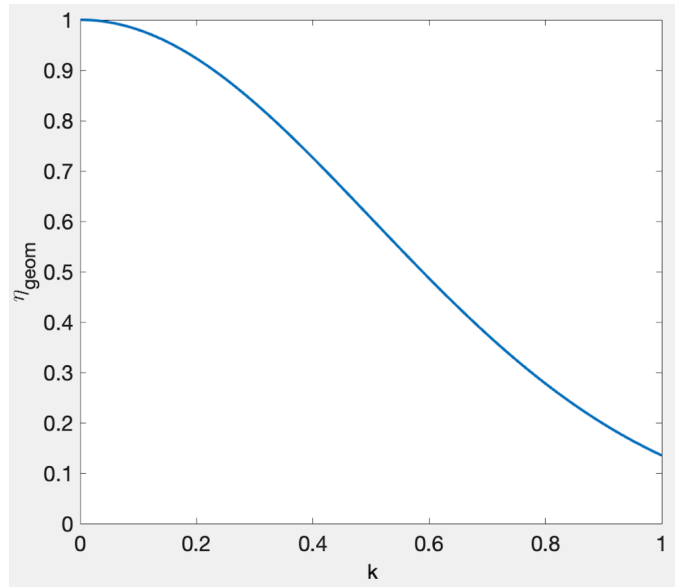


FIG. 3: η_{geom} expressed as a function of k .

B. The beams polarization

The most general situation that we can modelize in terms of polarization consists in two beams exiting the cavity, with elliptical polarizations, and a certain angle between the ellipses axes. The polarizations of the beams are elliptical if the cavity is not perfectly planar, and their ellipticity is connected to such non-planarity, as described in [6]. The angle (let's call it β) between the two polarization ellipses minor axes' (see Fig.4) could instead be due to a possible birefringence of the output mirror. Hence, we calculate the contribution to contrast caused by the scenario of the two polarizations, η_{pol} , starting from the calculations in [7], and considering the same direction of propagation for the two interfering beams. We remind that, for circular polarizations, it is, considering left-handed photons, without loss of generality:

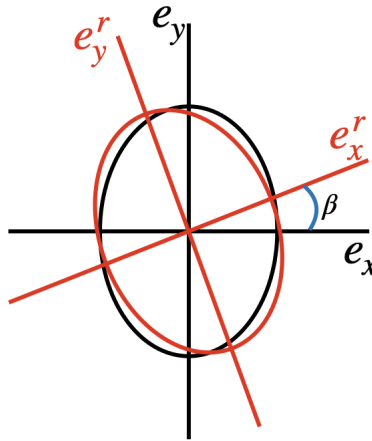


FIG. 4: Schematic representation of a possible rotation of the elliptical polarization, between the two interfering beams.

$$\eta_{pol} = |e_L \cdot e_L^*| = \frac{1}{2} |(e_x + ie_y) \cdot (e_x - ie_y)| = \frac{1}{2} (e_x^2 + e_y^2) = 1 \quad (11)$$

From the description of circular polarizations we can derive the description of elliptical polarizations, by introducing two different coefficients "a" and "b" that respectively multiply e_x and e_y , they represent the polarization ellipses' semi-axes; if the angle is null between the two ellipses minor axes, we have:

$$\eta_{pol} = \frac{1}{2}|(ae_x + ibe_y) \cdot (ae_x - ibe_y)| = \frac{1}{2}(a^2e_x^2 + b^2e_y^2) = \frac{1}{2}(a^2 + b^2) = 1, \quad (12)$$

which gives us a normalization condition for the semi-axes of a beam polarization ellipse. Now, if we introduce a non-zero angle between the axes of the ellipses that represent the polarizations of the counter-propagating beams, we can calculate again the contribution of polarizations to contrast; if we rotate the polarization ellipse of an angle β , in one of the two interfering beams, we can refer to the orthogonal versors e_x^r and e_y^r (fig.4), rotated of an angle β with respect to e_x and e_y , respectively; we have:

$$\begin{aligned} \eta_{pol} &= \frac{1}{2}|(ae_x + ibe_y) \cdot (ae_x^r - ibe_y^r)| = \\ &= \frac{1}{2}|a^2(e_x \cdot e_x^r) + b^2(e_y \cdot e_y^r) + iab(e_y \cdot e_x^r) - iab(e_x \cdot e_y^r)| = \\ &= \frac{1}{2}|(a^2\cos(\beta) + b^2\cos(\beta) + iab \cdot \cos(\frac{\pi}{2} - \beta) - iab \cdot \cos(\frac{\pi}{2} + \beta))| = \\ &= \frac{1}{2}|(a^2 + b^2)\cos(\beta) + iab \cdot \sin(\beta)| = \\ &= \sqrt{\frac{1}{4}(a^2 + b^2)^2 \cdot \cos^2(\beta) + a^2b^2 \cdot \sin^2(\beta)} = \\ &= \sqrt{\cos^2(\beta) + a^2b^2 \cdot \sin^2(\beta)}, \end{aligned} \quad (13)$$

the last equivalence is true because of the normalization condition given in Eq.(12), such condition also guarantees $\eta_{pol} \leq 1$, where the "equals" applies in the case $a = b = 1$, which leads back to circular polarization for both beams, and to Eq.(11). If $a = 0$ or $b = 0$, we are in the case of linear polarization for the two beams, and $\eta_{pol} = \cos(\beta)$.

III. MEASUREMENT OF THE BEAMS POLARIZATION STATES

For GP2, observations of the output beams polarizations were performed, following a procedure similar to the one described in [8]. The experimental setup utilized is the GP2 RLG prototype, at INFN-Pisa, shown in Fig.5. GP2 is a square RLG, 1.6 m side, an heterolythic active cavity; the area vector is oriented parallel to the Earth rotation axis, in order to obtain the maximum Sagnac frequency [5].

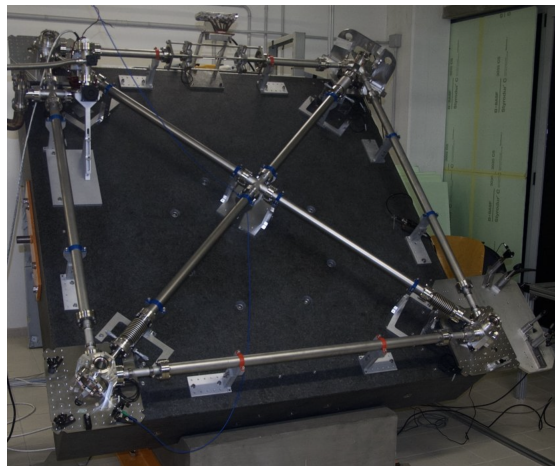


FIG. 5: Experimental setup with "GP2" RLG at INFN-Pisa.

A full reconstruction of the polarization ellipse, from the intensity measured as a function of the polarizer's angle, was performed. By means of a rotating polarizer and a photodiode, a polarization analysis has been performed

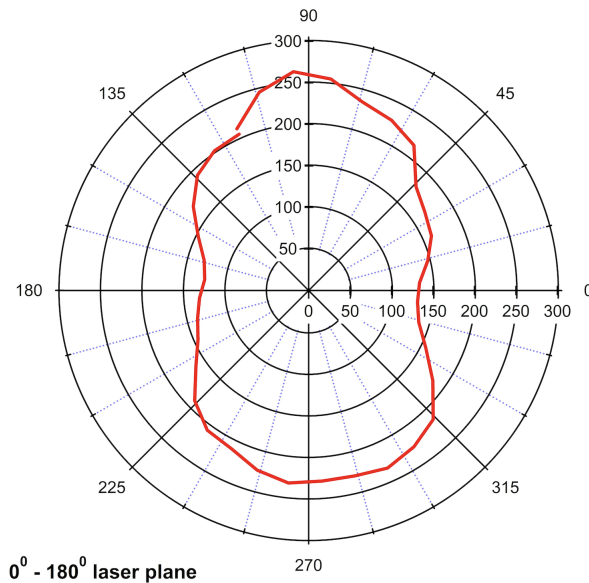


FIG. 6: Polar graph obtained by the polarization analysis on one of the two laser beams, in GP2. Light intensity with respect to the polarizers' angle is expressed in mV; 0° and 180° indicate the laser plane.

on the CCW beam. The resulting intensity polar graph (Fig.6) shows a peanut shape whose major to minor axes ratio is approximately 2:1, indicating an elliptical polarization with principal axes ratio 1.4:1. The major axis of the polarization ellipse is ccw rotated of an angle $\phi' = 44 \pm 17$ mrad with respect to the perpendicular to the laser plane.

According to [6], from the measurement of the beams' polarizations outside the cavity, it is possible to recover the polarization circulating in the ring laser cavity. First, with a dedicated experimental set-up we have measured the angular birefringence of a test mirror belonging to the same set of those mounted on GP2. A linearly polarized He-Ne laser beam (632.8 nm) is sent on the mirror at an angle of 45° and the mirror induced polarization rotation on the reflected beam is analyzed by means of a polarizer. The measurement is performed both for vertical (S-type) and horizontal (P-type) laser polarization obtaining a birefringence $\chi = 11 \pm 1$ mrad. For the same test mirror, we measured the values of the intensity transmission coefficients T_s and T_p for S and P incident polarized light, giving for the fields amplitudes ratio $t_s/t_p = (T_s/T_p)^{1/2} = 0.062 \pm 0.002$, and resulting in an amplitude anisotropy $\delta = 90 \pm 10$ ppm.

Following [6], when $\delta \ll \chi$ it is possible to calculate the out-of-plane misalignment angle α of the ring laser as:

$$\alpha \simeq \phi' \cdot \chi \frac{t_s}{t_p} \cdot \sqrt{2} \simeq (43 \pm 15) \text{ } \mu\text{rad} \quad (14)$$

We can conclude that the polarization circulating inside the ring cavity is approximately linear, the electric field components ratio given by:

$$\frac{E_p}{E_s} = \tan(\phi) \simeq \phi = \frac{\alpha}{\chi} \frac{1}{\sqrt{2}} \simeq 0.0028 \text{ } \text{mrad}. \quad (15)$$

IV. INTERFERENCE OF BEAMS WITH LINEAR AND ELLIPTICAL POLARIZATIONS, MEASUREMENTS AND COMPARISON

A. Measurements of observables and comparisons

The measurement is dedicated to understanding the impact of the interfering beams polarization on data quality; therefore, we compare the quality of the interference obtained with elliptically polarized beams outside the cavity (as measured and described in the previous paragraph) with quality obtained by making linear the polarizations of beams exiting the cavity. Two distinct beat note signals were acquired, in the two lower corners of the square gyroscope: in one corner, the elliptic polarization states were rotated with respect to each other in order to maximize contrast, in

the other corner the polarization states were made linear and then rotated in order to maximize the contrast; these operations were made by using $\lambda/2$ and $\lambda/4$ plates. In figure 7 the creation of the two beat notes between linearly and elliptically polarized interfering beams is shown.

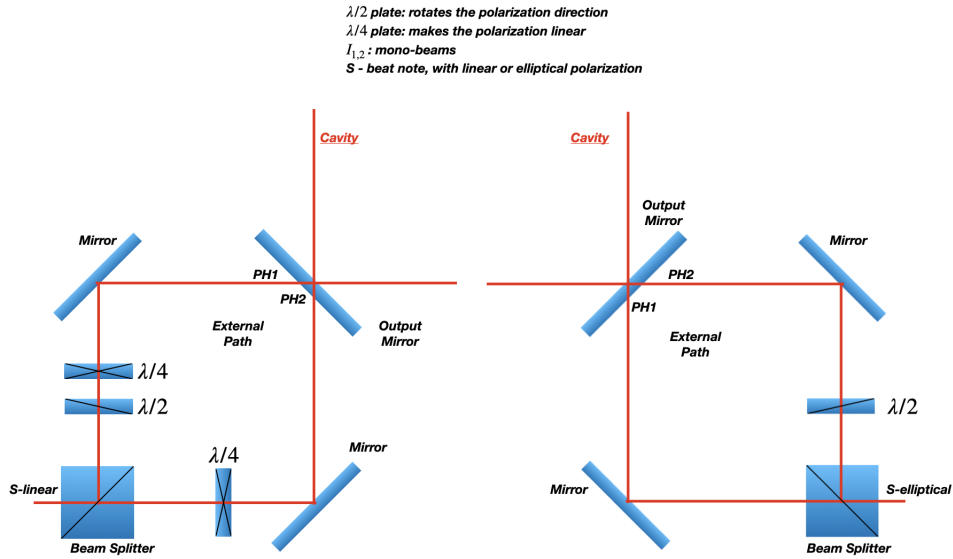


FIG. 7: Schematic view of the 2 corners of the GP2 RLG, where two beat note signals are created by interfering beams with elliptical and linear polarization states.

Data quality in the two acquisitions was evaluated on the basis of C and ω_m . In Fig. 8, we can see a comparison in contrast between beat note signals obtained with linearly and elliptically polarized interfering beams, on a portion of data chosen for its low noise level.

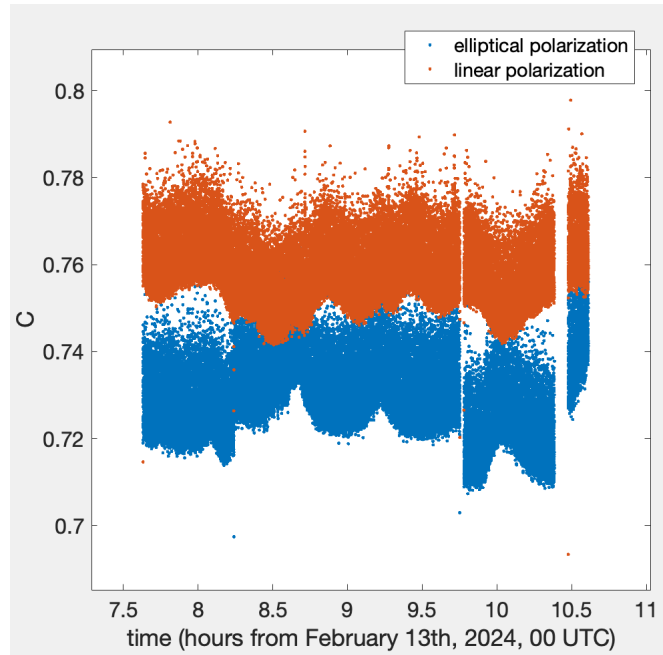


FIG. 8: Contrast of the beat note acquired in two different corners of the RLG, with elliptically (blue) and linearly (orange) polarized interfering beams.

The improvement, by obtaining an interference between linearly polarized beams, is evident. This can be explained by the model implemented for η_{pol} : in fig.9 η_{pol} vs β is shown, for beams with linear and elliptic polarizations, with

$\frac{a}{b} = 1.4$, in the second case, such ratio was measured between the axes of the polarization ellipse in GP2, as described in the previous paragraph. As we can observe, in case of linear polarizations, the variation of η_{pol} vs β is much sharper, with respect to the case of "almost circular" polarization ellipses. This means that, by utilizing linearly polarized beams, we have a better sensitivity to the polarizations rotations and alignment, and as a result it is easier to obtain identical polarization states in interfering beams.

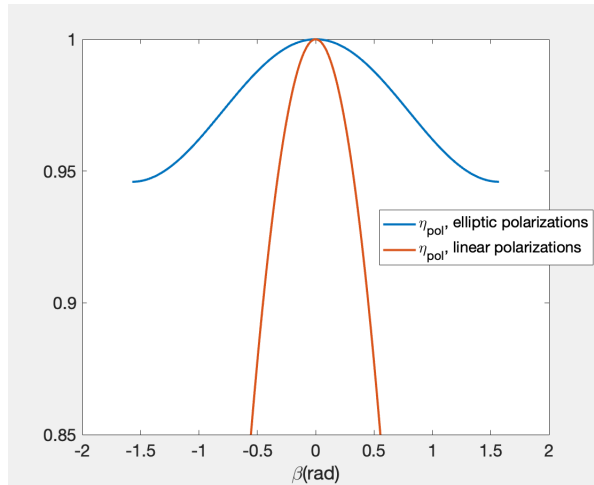


FIG. 9: η_{pol} vs β is shown, for beams with linear and elliptic polarizations, with $\frac{a}{b} = 1.4$.

C and ω_m parameters show that we can obtain better performances from a RLG where the beams are made linearly polarized before interfering, as shown in figure 10. In particular, $\sigma(\omega_m)$ is an indicator of the signal-to-noise ratio.

Polarizations	$\mu(contrast)$	$\sigma(contrast)$	$\sigma(\omega_m/2\pi)(Hz)$
Linear	0.761	0.0121	0.259
Elliptic	0.743	0.0134	0.265

FIG. 10: Parameters considered for comparing the performance of the RLG working with linearly or elliptically polarized interfering beams.

B. Measurement of the beams off axis

Utilizing data taken with linearly polarized beams, the η_{geom} factor of contrast was inferred, from Equations 5 and 6; we considered $\eta_{pol} \simeq 1$ in this case, and utilized the term including the beams intensities. Utilizing the model described in Eq.(10) and Figure 3, we first calculate the beams off-axis on selected "good data", in terms of the dimensionless parameter k , introduced in Paragraph 2.A, then we derive the beams off-axis.

The beam radius was measured by using a webcam Encore EN-WB-UHD01. The instrument registered the beam gaussian profile, and the result was $r = \sigma \cdot \sqrt{2} = 0.54 \pm 0.05$ mm, r is the beam radius at which the beam intensities fall to $1/e^2$ of their axial values. From the definition of k , we have, for the distance d , the beams off-axis:

$$d = 2 \cdot k \cdot r, \quad (16)$$

such quantity is shown in Fig. 11. Considering data taken on February 12th, 2024, and propagating the error on k and r , we obtain for the measurement of the beam off-axis $d = 0.40 \pm 0.07$ mm, at 3σ C.L.; it is reasonable to think the off-axis partially due to the cavity non-planarity estimated in Eq. (14).

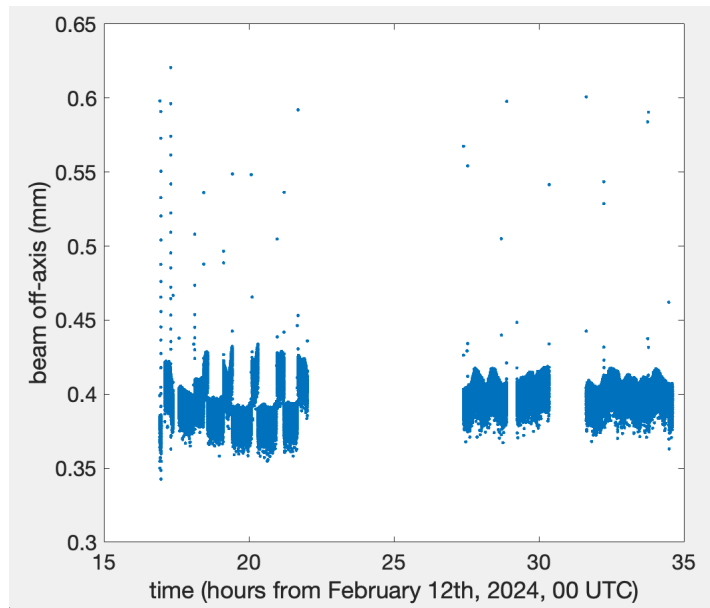


FIG. 11: Beams off-axis in mm, estimated from linearly polarized beams interference

V. CONCLUSIONS

An active heterolythic Ring Laser Gyroscope was characterized, in its planarity, alignment and beams polarization. The fringe contrast was factorized in terms of beams ratio, geometrical alignment of the square cavity, and beams polarization. Models were implemented for the contribution of alignment and beams polarization to contrast. Measurements were taken with linearly and elliptically polarized beams, and compared. As a result, operating an RLG with linearly polarized interfering beams appears to be more convenient, in terms of fringe contrast, and signal-to-noise ratio. An estimation of the beams off-axis was performed, exploiting the estimation of the other factors contributing to fringe contrast.

VI. DISCLOSURES

The authors declare no conflicts of interest.

VII. FUNDING

We acknowledge the "Istituto Nazionale di Fisica Nucleare" for funding the experiment.

-
- [1] A. Basti et al., "GINGER data analysis for seismology", submitted Oct 30, 2023, to "Annals of Geophysics", submission n. 9033
 - [2] Di Somma, G.; Altucci, C.; Bajardi, F.; Basti, A.; Beverini, N.; Capozziello, S.; Carelli, G.; Castellano, S.; Ciampini, D.; De Luca, G.; et al. Possible Tests of Fundamental Physics with GINGER. *Astronomy* 2024, 3, 21–28. <https://doi.org/10.3390/astronomy3010003>
 - [3] A. Di Virgilio, N. Beverini, G. Carelli D. Ciampini, F. Fuso, E. Maccioni, Analysis of ring laser gyroscopes including laser dynamics, *Eur. Phys. J. C* 79: 573 (2019) <https://doi.org/10.1140/epjc/s10052-019-7089-5>
 - [4] A.D.V. Di Virgilio, N. Beverini, G. Carelli, D. Ciampini, F. Fuso, U. Giacomelli, E. Maccioni, A. Ortolan: Identification and correction of Sagnac frequency variations: an implementation for the GINGERINO data analysis, *Eur. Phys. J. C* 80:163 (2020) <https://doi.org/10.1140/epjc/s10052-020-7659-6>
 - [5] E.Maccioni et al., High sensitivity tool for geophysical applications: a geometrically locked ring laser gyroscope, *Applied Optics* Vol. 61, Issue 31, pp. 9256-9261 (2022) <https://doi.org/10.1364/AO.469834>

- [6] H.R. Bilger, G.E. Stedman and P.V. Wells, "Geometrical dependence of polarisation in near-planar ring lasers", OPTICS COMMUNICATIONS (1990) Vol.80, n.2, Pages 133-137
- [7] L.Z. Cai, X.L. Yang, "Interference of circularly polarized light: contrast and application in fabrication of three-dimensional periodic microstructures", Optics & Laser Technology 34 (2002) 671 – 674
- [8] Ramonika Sengupta, Brijesh Tripathi, and Asha Adhiya, "Explicit Reconstruction of Polarization Ellipse using Rotating Polarizer", arXiv:2211.15244